SHG of Ultrathin Films of Metal Porphyrins on BK7 Glass in Total Internal Reflection Geometry: Theory and Experiments

Lorenzo Echevarria,* Pedro Nieto, Héctor Gutiérrez, Vladimiro Mújica, and Manuel Caetano*

Universidad Central de Venezuela, Facultad de Ciencias, Escuela de Química, Apartado 47102, Caracas 1020A, Venezuela

Received: December 28, 2002; In Final Form: June 13, 2003

We present a novel methodology that combines a theoretical description and experimental characterization of the structure and first hyperpolarizability of ultrathin films of VO-octaethyl-porphyrins (VOOETP, Scheme 1) adsorbed on a BK7 activated glass. Films were characterized by ellipsometry, and the geometry is inferred from a consistent comparison between the theoretical hyperpolarizability and the experimental measurements. The hyperpolarizability is determined through second harmonic generation (SHG) techniques, and ellipsometry is used independently to determine the thickness of the film. An analysis of the Fourier components of the tensor relating the incident and SHG fields reveals the existence of a linear dependence between the Fourier components that greatly reduces the amount of required experimental information. Using this methodology, we obtain reasonable agreement between the observed and calculated intrinsic hyperpolarizabilities ($\beta_z^{exp}/\beta_z^{theo} = 0.95$) that we attribute to the dimer.

1. Introduction

The optical response of thin films of optically active molecules adsorbed on a surface depends to a large extent on the surface dipole moment created as a consequence of charge-transfer processes. This is a highly system-dependent phenomenon that is influenced, among other factors, by surface coverage and eventual aggregation processes.

Metal porphyrins have been widely studied because of their potential for use in optoelectronic devices.[1,2] In heavy and extra-heavy oils, vanadium and nickel porphyrins are important components, and an understanding of molecular interactions in these compounds and their role in influencing aggregation processes may be of importance in improving the extraction and transport of crude.[3]

SHG is a powerful tool for the study of equilibrium and dynamical processes in interfaces because of its ability to respond to noncentrosymmetric environments. The signal vanishes for liquids, gases, and solids with centers of symmetry but is nonzero for boundary-like systems (e.g., solid−air, solid−liquid, liquid−vapor, and liquid−liquid interfaces).[4−6]

Semiempirical electronic structure calculations of porphyrinic systems have proved to be very valuable in systematizing the influence of chemical substituents on the optical properties of extended systems. Particularly relevant to our work is the study of Marks and co-workers where the effect of transition metals is deemed comparable to that of organic chromophores in enhancing optical response.[7]

A consistent model to correlate the theory and experiment on SHG of adsorbed species hinges on a number of specifications of the conditions of the measurements, the geometry of the interface, and the relationship between the measured susceptibility and the calculated hyperpolarizability. These two tensors are related through a rotational transformation whose specific form depends on a consistent treatment of the theoretical model and the experimental information. This article is organized as follows: Section 1 presents the relevant theory for the calculation of the hyperpolarizability tensor. Section 2 describes the treatment of the experimental measurements of the susceptibility to obtain the hyperpolarizability. Section 3 presents the results for various models of the VOOETP system. Finally, section 4 contains a critical appraisal of the model and some final considerations.

SCHEME 1: VOOETP Structure

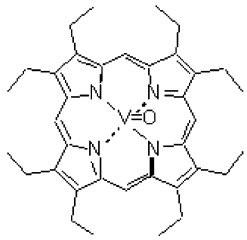

2. Theory

Our approach to calculating the hyperpolarizability of the adsorbate−surface complex is an extension of the hybrid quantum classical methodology that we employed in the description on the interaction between radical and asphaltene fragments.[8] The surface is represented by a cluster of SiO_2, and the geometry of the molecule−cluster system is determined using the universal force field,[9,10] a molecular mechanics-based method. A semiempirical quantum chemical calculation of the electronic structure of the complex is then used to compute the hyperpolarizability as a sum over states.

2.1. Structure of Octaethyl-Porphirines and Semiempirical Parameters. The structure of VO-octaethyl-porphirines has been established by X-ray diffraction.[11] This result gives a value of 0.543 Å for the distance from the plane to the VO group and 1.620 Å for the V−O bond length. Theoretical studies of Zerner and Gouterman[12] using an all-valence-orbitals version of the extended Hückel method predict that the VO group in VOOETP is out of the plane formed by the pyrrolic nitrogen atoms (Scheme 1).

* Corresponding authors. E-mail: lechevar@ciens.ucv.ve. Phone: 58-212-6051260. Fax: 58-212-605124. E-mail: mcaetano@ciens.ucv.ve. Phone: 58-212-6051216. Fax: 58-212-6051246.

10.1021/jp027843s CCC: $25.00
Published on Web 08/08/2003

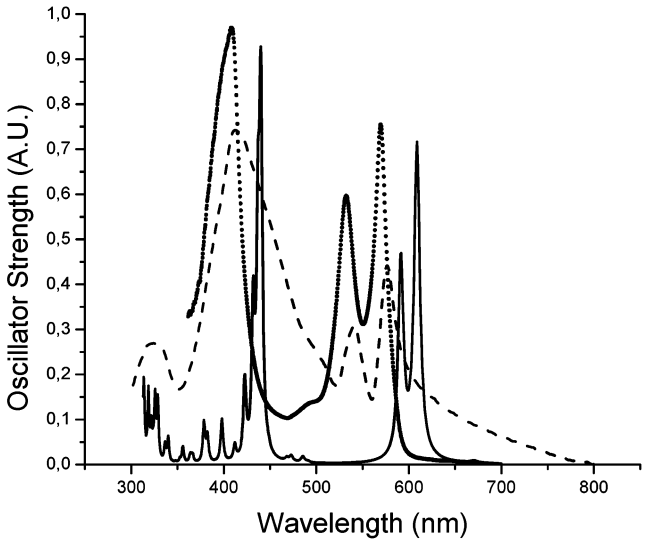

Figure 1. Theoretical and experimental absorption spectra: (—) theoretical, (- - -) Surface and (···) Solution.

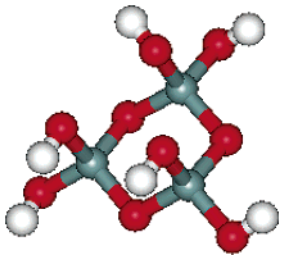

Figure 2. SiO_2 cluster geometry.

A consistent description of the electronic description of an open-shell system such as VOOETP ($3d^1$) cannot be achieved with the standard parameters for INDO/S. In particular, there are two parameters, f_σ and f_π, related to orbital overlap, which must be reoptimized. The situation resembles that encountered by Mujica et al. in the description of radical−molecule interactions when using the standard values of these parameters: 0.585 and 1.267, respectively. There the optimization was based on an energy criterion, whereas in our case we have chosen the parameters to reproduce the electronic spectrum.

Such a procedure leads to values of 2.640 and 0.100, which result in a much larger weight of the π factor, thereby providing a better description of the VO-porphynate. Similar to metalporphyrins, the absorption spectrum of VOOETP presents a number of characteristic bands:[13] two bands (Q) in the visible region between 500 and 600 nm; one band (a Soret or B band) located between 380 and 420 nm; a group of lower-energy bands (N, L, M) blue-shifted from the Soret band and generally located around 325 nm (N), 215 nm (M), and the L band, of lower intensity, between the other two. Figure 1 shows general agreement between these experimental and calculated spectral features.

To validate the use of the cluster shown in Figure 2, we have calculated the porphyrin-surface anchoring angle (Figure 3), esssentially determined by the interaction VO···H−O−Si≡, and have found that our level of calculation fits the experimentally determined angle as seen in Table 1 for the monomer and the dimer.

2.2. First Hyperpolarizability. We have adopted a methodology proposed by Marks, Ratner, and co-workers[14,15] for the calculation of the first molecular hyperpolarizability, β. First, we calculate the ground and excited SCI states of VOOETP

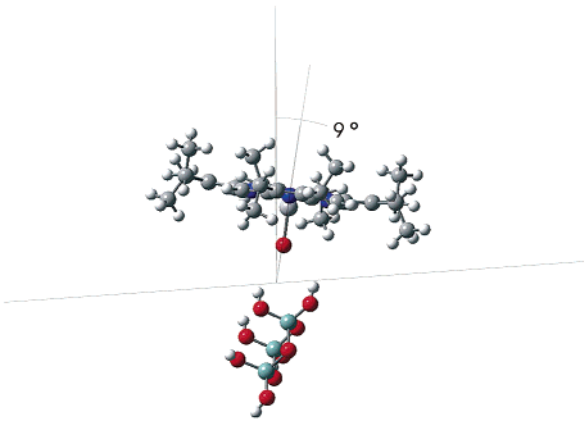

Figure 3. View of the VOOETP/SiO_2 anchoring.

TABLE 1: Hyperpolarizability and Geometrical Parameters for Different Systems[a]

d (nm)	θ_0 (deg)	N[b]	$\rho(\theta_0)$[c]	χ_1[d]	β_z^{exp}	β_z^{theo}
0.9 ± 0.3	9.5	1	3.8	7.2 ± 0.2	6.8	1.6
1.8 ± 0.3	13.4	2	5.5	3.4 ± 0.2	2.0	1.9

[a] The values of β are expressed as ($\times 10^{-29}$ esu). [b] $N = (2d\ (\cos \theta_0))/A^{1/2}$where A the is theoretical molecular contact surface given by Cerius. [c] Molecular density in ($\times 10^{14}$ molecules/cm^2). [d] Susceptibility in ($\times 10^{-14}$ esu).

for the experimental geometry (C_{2v}), and then β is computed as a sum over states (SOS). The required electronic states are calculated at the ROHF level using the code ZINDO Cerius^2, version 4 of msi.[16] Trsic et al. have used the same level of calculation[17] in their study of porphyrinic dimers. Because of computational limitations, we have considered only the singlet configuration of the dimer of VOOETP. For the closed-shell systems, a similar methodology is employed but at the RHF level. The SOS[18] expression, originally derived by Ward,[19] has the explicit form

$$\beta_{ijk}^{SHG} = -\frac{e^3}{8h^2}\sum_{n\neq g}\sum_{\substack{g'\neq g\\ n'\neq n}}\sum (r^{j}_{gn'} r^{i}_{n'n} r^{k}_{gn} + r^{k}_{gn'} r^{i}_{n'n} r^{j}_{gn}) \left(\frac{1}{(\omega_{n'g}-\omega)(\omega_{ng}+\omega)} + \frac{1}{(\omega_{n'g}+\omega)(\omega_{ng}-\omega)}\right)$$
$$+ (r^{i}_{gn'} r^{j}_{n'n} r^{k}_{gn} + r^{i}_{gn'} r^{k}_{n'n} r^{j}_{gn}) \left(\frac{1}{(\omega_{n'g}+2\omega)(\omega_{ng}+\omega)} + \frac{1}{(\omega_{n'g}-2\omega)(\omega_{ng}-\omega)}\right)$$
$$+ (r^{j}_{gn'} r^{i}_{n'n} r^{k}_{gn} + r^{k}_{gn'} r^{i}_{n'n} r^{j}_{gn}) \left(\frac{1}{(\omega_{n'g}-\omega)(\omega_{ng}-2\omega)} + \frac{1}{(\omega_{n'g}+\omega)(\omega_{ng}+2\omega)}\right) \quad (1)$$
$$+ 4\sum_{n\neq g}\left\{\left[r^{j}_{gn} r^{k}_{gn} \Delta r_n^{\,i}(\omega_{ng}^2 - 4\omega^2) + r^{i}_{gn}(r^{k}_{gn} \Delta r_n^{\,j} + r^{j}_{gn} \Delta r_n^{\,k})\right.\right.$$
$$\left.\left.(\omega_{ng}^2 - 2\omega^2)\frac{1}{(\omega_{ng}^2-\omega^2)(\omega_{ng}^2-4\omega^2)}\right]\right\}$$

Here ω is the frequency of the applied field, $r^{i}_{n'n} = \langle \Psi_{n'} | \mathbf{r}^i | \Psi_n \rangle$ are the matrix elements of the displacement operator along the ith molecular axis between the electronic states $\Psi_{n'}$

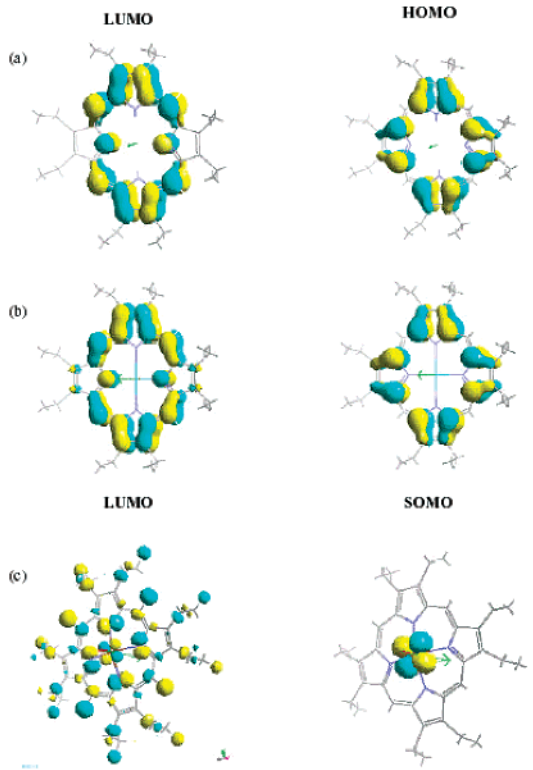

Figure 4. SOMO and LUMO molecular orbitals for gas-phase VOOETP.

and Ψ_n, $\hbar\omega_{ng}$ is the energy separation between the ground and the nth excited state Ψ_n, and $\Delta r_n^i = r_{nn}^i - r_{gg}^i$ is the difference between the dipole moments of the same states. By using the above-described methodology, we find that for VOOETP the only nonvanishing element of the hyperpolarizability tensor for the isolated molecules is β_{zzz}. Similar calculations for the other analogous structures (NiOETP, OETP) give $\beta_{xxz} = \beta_{xzx}$ and β_{zxx} different from zero.

Once the tensor components of β have been obtained, one can calculate the diagonal intrinsic components along the axis of the molecular reference system as[20]

$$\beta_i = \beta_{iii} + \frac{1}{3}[\sum_{j\neq i}(\beta_{ijj} + \beta_{jij} + \beta_{jji})] \qquad i,j = x,y,z \quad (2)$$

These components are used to determine the vector component along the dipole moment direction β_{vec}, which is the quantity sampled experimentally:

$$\beta_{vec} = \sum_{i=1}^{3} \frac{\mu_i \beta_i}{|\mu|} \quad (3)$$

$\vec{\mu} = (\mu_x, \mu_y, \mu_z)$ is the dipole moment operator. One can also define the nondirectional quantity

$$\beta_T = \sqrt{\beta_x^2 + \beta_y^2 + \beta_z^2} \quad (4)$$

which is the one that is actually used to compare theory and experiment.

We see that this magnitude increases in the order OETP < NiOETP < VOOETP. This effect is clearly related to the fact that VOOETP is an open-shell system, which in turn translates into an increased ability to transfer charge from the metal to the ligand (MLCT).[21] This is also evident in Figure 4, which shows that the HOMO and LUMO orbitals of the reference porphyrin (OETP) and the Ni-substituted species share a common localization pattern (Figure 4a and b). This is in sharp contrast to the situation for VOOETP (Figure 4c), where the SOMO is largely localized over the vanadium whereas the LUMO is distributed along the porphynate ligand.

3. Field Propagation in a Prism and the SHG Signal

The incident field with frequency ω propagates perpendicularly to the face of the prism opposite to the one where the sample is adsorbed, where the beam is totally reflected. The evanescent wave interacts nonlinearly with the adsorbate,[22] producing the SHG signal at frequency 2ω that goes through the prism and is detected on exiting. Using the reference system proposed by Felderhof and collaborators,[23] we can write the transmission coefficient through the prism's faces for the incoming and outgoing fields at frequencies ω and 2ω as

$$t_{IN} = \frac{2}{1 + n(\omega)} \qquad t_{OUT} = \frac{2n(2\omega)}{n(2\omega) + 1} \quad (5)$$

where $n(\omega)$ and $n(2\omega)$ are the indices of refraction at the fundamental and second harmonic frequencies, respectively. The linear f_X, f_Y, f_Z and nonlinear F_X, F_Y, F_Z Fresnel factors are given by

$$f_X = \frac{2n(\omega)\sqrt{1 - {}^1/_2 n(\omega)^2}}{1 - n(\omega)\sqrt{2 - n(\omega)^2}} t_{IN}$$

$$f_Y = \frac{2n(\omega)}{n(\omega) - \sqrt{2 - n(\omega)^2}} t_{IN} \quad (6)$$

$$f_Z = -f_X$$

$$F_X = \frac{n(2\omega)\sqrt{1 - {}^1/_2 n(\omega)^2}}{\sqrt{n(2\omega)^2 - {}^1/_2 n(\omega)^2} - n(2\omega)^2\sqrt{1 - {}^1/_2 n(\omega)^2}}$$

$$F_Y = \frac{1}{\sqrt{n(2\omega)^2 - {}^1/_2 n(\omega)^2} - {}^1/_2\sqrt{1 - {}^1/_2 n(\omega)^2}} \quad (7)$$

$$F_Z = \frac{2n(2\omega)n(\omega)}{\sqrt{2n(2\omega)^2 - n(\omega)^2} - n(2\omega)^2\sqrt{2 - n(\omega)^2}}$$

The relevant polarization response in SHG is given in terms of a third-rank susceptibility tensor $\chi^{(2)}$ that relates the polarization to products of the incident and response fields. If the film is assumed to be isotropic in the $(X-Y)$ plane defined by the surface of the prism and presents inversion symmetry in the same plane (case I), then the third-rank susceptibility tensor that can be written in matrix form as

$$\chi = \begin{bmatrix} 0 & 0 & 0 & 0 & \chi_{XZX} & 0 \\ 0 & 0 & 0 & \chi_{XZX} & 0 & 0 \\ \chi_{ZXX} & \chi_{ZXX} & \chi_{ZZZ} & 0 & 0 & 0 \end{bmatrix} \quad (8)$$

The experimental determination of the susceptibility tensor is done indirectly through a measurement of the components of the polarization parallel (p) and perpendicular (s) to the plane

of incidence. The incident and SHG fields are related by[23]

$$\begin{pmatrix} E_R^p(2\omega) \\ E_R^s(2\omega) \end{pmatrix} = \begin{pmatrix} a_{ppp} & a_{pss} & 0 \\ 0 & 0 & a_{sps} \end{pmatrix} \begin{pmatrix} E_I^{p^2}(\omega) \\ E_I^{s^2}(\omega) \\ E_I^p(\omega)\, E_I^s(\omega) \end{pmatrix} \tag{9}$$

The reduced tensor components a_{abc} in (s, p) coordinates are related to the susceptibility tensor $\chi^{(2)}_{IJK}$ in (X, Y, Z) coordinates by[23]

$$\begin{aligned} a_{ppp} &= 8\pi ik[2F_X f_X f_Z \chi_{XZX} + F_Z(f_X^2 \chi_{ZXX} + f_X^2 \chi_{ZZZ})] \\ a_{pss} &= 8\pi ikF_Z f_Y^2 \chi_{ZXX} \\ a_{sps} &= 16\pi ikF_Y f_Y f_Z \chi_{XZX} \end{aligned} \tag{10}$$

Once the SHG field passes through a polarizer rotated by an angle ζ with respect to its principal axis, it can be written as

$$\mathbf{E}^{2\omega}_{R,\zeta} = E_R^p(2\omega)\cos\zeta + E_R^s(2\omega)\sin\zeta \tag{11}$$

and its intensity, relative to the intensity of the incident radiation, is

$$R_\zeta(\varphi) = \frac{I^{2\omega}_{\zeta\mathrm{OUT}}}{I^{\omega}_{\mathrm{IN}}} = \frac{|\mathbf{E}^{2\omega}_{R,\zeta}(\varphi)|^2}{|\mathbf{E}^{\omega}_I|^2} \tag{12}$$

Determining the real and imaginary part of $\chi_S^{(2)}$ requires a separate analysis of the SHG and the incident radiation on the polarization angle. To this end, a fourth-wave retarding device was introduced in the optical path to modify the polarization of the fundamental incident radiation by an angle φ.

After passing through the retarding device, the incident electric field polarized in the p direction has the following components:

$$E_I^{\,p} = \frac{1}{\sqrt{2}}E_I(i + \cos 2\varphi) \qquad E_I^{\,s} = \frac{1}{\sqrt{2}}E_I \sin 2\varphi \tag{13}$$

The standard way to determine the components of the tensor $a_{abc} = Re\{a_{abc}\} + iIm\{a_{abc}\}$ involves doing a Fourier analysis of the intensity ratios $R_\zeta(2\omega, \varphi)$ in eq 8 for four different values: $\zeta = 0$, 45, 90, and 135°.[24] One can evidently write eq 12 as

$$R_\zeta(\varphi) = \sum_{m=0}^{4}[C_{m,\zeta}\cos m2\varphi + S_{m,\zeta}\sin m2\varphi] \tag{14}$$

where the Fourier coefficients $C_{m,\zeta}$ and $S_{m,\zeta}$ are given by

$$C_{0,\zeta} = \frac{2}{\pi}\int_0^{\pi/2} R_\zeta(\varphi)\, \mathrm{d}\varphi \tag{15}$$

$$C_{i,\zeta} = \frac{4}{\pi}\int_0^{\pi/2} R_\zeta(\varphi)\cos(m\varphi)\, \mathrm{d}\varphi \tag{16}$$

$$S_{i,\zeta} = \frac{4}{\pi}\int_0^{\pi/2} R_\zeta(\varphi)\sin(m\varphi)\, \mathrm{d}\varphi \tag{17}$$

and the dependence on angle φ has been made explicit.

The relationship between the intensity ratios, the reduced tensor a_{abc}, and the incident radiation components can be obtained from eqs 9, 11, 12, and 13:

$$\begin{aligned} R_{0°}(\varphi) &= |a_{ppp}E_I^{p^2} + a_{pss}E_I^{s^2}|^2 \\ R_{90°}(\varphi) &= |a_{sps}E_I^p\, E_I^s|^2 \\ R_{45°}(\varphi) &= \frac{1}{2}|a_{sps}E_I^p\, E_I^s + a_{ppp}E_I^{p^2} + a_{pss}E_I^{s^2}|^2 \\ R_{135°}(\varphi) &= \frac{1}{2}|a_{sps}E_I^p\, E_I^s - a_{ppp}E_I^{p^2} - a_{pss}E_I^{s^2}|^2 \end{aligned} \tag{18}$$

An analysis of the obtained Fourier coefficients in this case reveals a linear dependence between the coefficients that has been overlooked in the reviewed literature:

$$C_{i,0°} + C_{i,90°} = 2C_{i,45°} \qquad \text{with } i = 0, 1, 2, 3, 4 \tag{19}$$

This simple expression implies a drastic reduction of the number of measurements required to determine and analyze the SHG signal because it implies that the information contained in the measurements at ζ equal to 0 and 90° is already present in the results for 45°, which would then be sufficient to determine the values of all of the tensor components $a_{abc} = Re\{a_{abc}\} + iIm\{a_{abc}\}$ and, consequently, the components of the susceptibility tensor.

Another interesting case under consideration (case II) is defined by the assumption that the film is isotropic in the plane $(X-Y)$ but lacks inversion symmetry with respect to the same plane. For this situation, the susceptibility tensor is given by

$$\chi = \begin{bmatrix} 0 & 0 & 0 & \chi_{XYZ} & \chi_{XZX} & 0 \\ 0 & 0 & 0 & \chi_{XZX} & -\chi_{XYZ} & 0 \\ \chi_{ZXX} & \chi_{ZXX} & \chi_{ZZZ} & 0 & 0 & 0 \end{bmatrix} \tag{20}$$

To take the symmetry into account, eq 9 must be modified to include the additional components and the equations for the

$$\begin{aligned} a_{spp} &= -16\pi ikF_Y f_X f_Z \chi_{XYZ} \\ a_{pps} &= 16\pi ikF_X f_Y f_Z \chi_{XYZ} \end{aligned} \tag{21}$$

$$\begin{pmatrix} E_R^p(2\omega) \\ E_R^s(2\omega) \end{pmatrix} = \begin{pmatrix} a_{ppp} & a_{pss} & a_{pps} \\ a_{spp} & 0 & a_{sps} \end{pmatrix} \begin{pmatrix} E_I^{p^2}(\omega) \\ E_I^{s^2}(\omega) \\ E_I^p(\omega)E_I^s(\omega) \end{pmatrix} \tag{22}$$

SHG response are consequently modified as

$$\begin{aligned} R_{0°}(\varphi) &= |a_{ppp}E_I^{p^2} + a_{pss}E_I^{s^2} + a_{pps}E_I^p\, E_I^s|^2 \\ R_{90°}(\varphi) &= |a_{spp}E_I^{p^2} + a_{sps}E_I^pE_I^s|^2 \\ R_{45°}(\varphi) &= \frac{1}{2}|a_{spp}E_I^{p^2} + a_{sps}E_I^p\, E_I^s + a_{ppp}E_I^{p^2} + a_{pss}E_I^{s^2} + a_{pps}E_I^p\, E_I^s|^2 \\ R_{135°}(\varphi) &= \frac{1}{2}|a_{spp}E_I^{p^2} + a_{sps}E_I^p\, E_I^s - a_{ppp}E_I^{p^2} - a_{pss}E_I^{s^2} - a_{pps}E_I^p\, E_I^s|^2 \end{aligned} \tag{23}$$

In this case, the relations, analogous to eq 19, between the Fourier coefficients corresponding to values of the polarization angle of 45, 0, and 90° are

$$\frac{C_{i,0°} + C_{i,90°}}{2} + \ldots = C_{i,45°} \qquad \frac{S_{i,0°} + S_{i,90°}}{2} + \ldots = S_{i,45°} \qquad \text{with } i = 0, 1, 2, 3, 4 \tag{24}$$

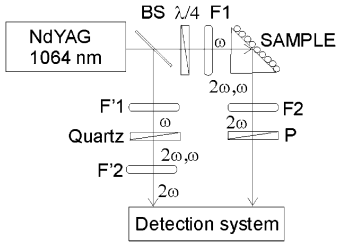

Figure 5. Experimental setup.

In the summation in eq 24, we have displayed only the relevant terms for the determination of the tensor $a_{abc} = Re\{a_{abc}\} + iIm\{a_{abc}\}$; the remaining terms can be determined using the same information.

4. Experimental Section

Figure 5 shows the experimental setup. The source is a Nd:YAG pulsed laser (Continuum, modelo Surelite I) that emits nanosecond pulses at 1064 nm with a surface density energy of 8 mJ/cm^2, and the polarization of the incident pulses is controlled with a $^{\lambda}/_{4}$ retarder. The radiation goes through a set of filters that remove wavelengths other than 1064 nm. The sample is supported on an optical-quality glass prism. The fundamental radiation is simultaneously transmitted through a quartz crystal to produce a reference beam in order to normalize the SHG signal.

Films are prepared by dropping diluted solutions of VOOETP in dichloromethane on the activated glass surface. To ensure an adequate surface concentration of −OH groups, we use a tested methodology to fabricate self-assembled films.[25−27] The width and homogeneity of the film is determined through ellipsometric measurements.[28,29] The fundamental radiation is disposed normal to the entry face of the prism to guarantee total internal reflection on the face where the sample is adsorbed. The SHG radiation is directed to a polarizer to select the desired component before arriving at the detection system. A system of filters are arranged at the exit of the Glan−Thompson polarizer to eliminate any residual fundamental radiation that may contaminate the SHG signal, which is detected by a Hammamatsu R955 photomultiplier in a spectrometer and averaged in a boxcar (Stanford Research Instruments, SR 250).

5. Comparison between Theoretical and Experimental Results

It is not possible, in general, to carry out a straightforward comparison between the measured and calculated susceptibilities because the experiment does not provide direct information about the orientation of the molecules on the surface. Rather, information about the geometry is extracted from theoretical calculations and is then used to obtain the experimental hyperpolarizability, something that can be directly compared to the theoretical results.

The basic assumption used in this comparison is that the susceptibility tensor can be written as a geometric transformation of the hyperpolarizabity tensor, where the geometric part of this expression is the same for the experimental and theoretical magnitudes (i.e., $\chi_{\text{theory}} = \mathbf{S}\beta_{\text{theory}}$ and $\chi_{\text{experiment}} = \mathbf{S}\beta_{\text{experiment}}$). This is a very reasonable assumption that allows us, using a given level of theoretical modeling, to compute the matrix **S**. Figure 6 displays a flowchart that makes explicit, in a schematic way, the various steps involved in the comparison of the calculated and experimental hyperpolarizabilities.

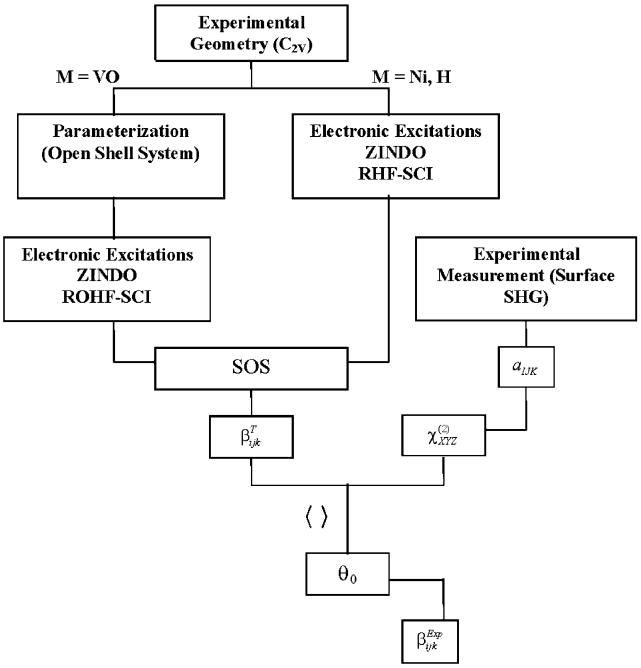

Figure 6. Schematic flowchart for the theory−experiment comparison.

5.1. Calculation of the Average Orientation. As explained above, the calculation of an approximated orientation starting from the experimental measurements of the susceptibility requires knowing which components of the tensor in the isolated molecule respond to the applied field. One can write the explicit relationship between the susceptibility in the laboratory system of reference (*I*, *J*, *K*) and the hyperpolarizability in the (*i*, *j*, *k*) molecular reference system as[30]

$$\chi^{(2)}_{IJK} = \langle \mathrm{d}(\phi, \theta, \psi)\, D_{Ii} D_{Jj} D_{Kk} \rangle \beta_{ijk} \tag{25}$$

where d(ϕ, θ, ψ) is a distribution function and D_{lm} are the director cosines, which can be expressed in terms of the Euler angles (ϕ, θ, ψ), where ϕ is the rotation angle about a normal to the surface, ψ is the rotation angle about the molecular axis, and θ is the angle between these two axes. The symbol $\langle\ \rangle$ indicates an orientational average, and the simplest distribution function d(ϕ, θ, ψ) is obtained under the assumption that the molecules are randomly distributed on the surface plane (i.e., intermolecular interactions are neglected). If we furthermore assume that molecules are symmetric with respect to the molecular axis then the θ part of the distribution function becomes a δ function.

Equation 25 can be rewritten so that the general connection between χ and β is made explicit:

$$\chi^{(2)}_{IJK}{}' = \sum_{i=1}^{3}\sum_{j=1}^{3}\sum_{k=1}^{3} D_{Ii} D_{Jj} D_{Kk} \beta_{ijk} \tag{26}$$

The index correspondence between the axis and index is $x = 1$ and 2, $z = 3$ for both coordinate systems. The orientational average is carried out as described above:

$$\langle \chi^{(2)}_{IJK} \rangle = \frac{1}{4\pi} \int_0^{\pi} \int_0^{2\pi} \int_0^{2\pi} \delta(\theta - \theta_0)\, \chi^{(2)}_{IJK}{}'\, \mathrm{d}\theta\, \mathrm{d}\psi\, \mathrm{d}\phi \tag{27}$$

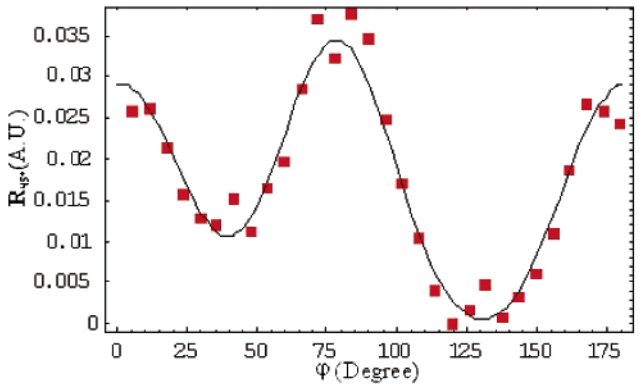

Figure 7. Rotational pattern of the SHG signal.

Because the only nonzero element is β_{zzz} (VOOETP case), we find the expressions for the tensor components of the susceptibility as functions of θ_0 and β_{zzz}:

$$\chi^{(2)}_{ZZZ} = \pi \cos^2\theta_0 \beta_{zzz} \tag{28}$$

$$\chi^{(2)}_{ZXX} = \frac{1}{2}\pi \cos\theta_0 \sin^2\theta_0 \beta_{zzz} \tag{29}$$

Dividing eq 28 by eq 29 leads to

$$\frac{\chi^{(2)}_{ZXX}}{\chi^{(2)}_{ZZZ}} = \frac{1}{2}\tan^2\theta_0 \tag{30}$$

If the nonzero tensor components are

$$\beta_{xxz} = \beta_{xzx}, \beta_{zxx}$$

(i.e., NiOETP, OETP), then the ratio of tensor components is given by

$$\frac{\chi_{ZXX}}{\chi_{ZZZ}} = \frac{(3 + \cos(2\theta_0))\csc^2(\theta_0)\beta_{zxx} - 4\beta_{xxz}}{4(2\beta_{xxz} + \beta_{zxx})} \tag{31}$$

6. Results

6.1. Experimental Determination of β. As discussed previously, the determination of β requires the obtaining of tensor components $a_{\alpha\beta\gamma}$. In Figure 7, the normalized response obtained with the analyzer at 45° is shown (eqs 12 and 23). A Fourier analysis of these data was realized, and by taking into account the relationship between the Fourier components for the case where inversion symmetry is absent (case II, eq 20), it is possible to determine the real and imaginary parts of $a_\alpha\beta\gamma$ as expressed by eqs 10 and 21. The equations describing the quartz signal are taken from the literature,[31] and the nonlinear coefficient of quartz (0.3 pm/V) is the most recently reported value.[32]

To compare the experimental and theoretical responses, we adopt the following convention that relies on the imposed system symmetry and is independent of the reference system used:

$$\chi_X = 0$$
$$\chi_Y = 0 \tag{32}$$
$$\chi_Z = \chi_{ZZZ} + \frac{1}{3}(\chi_{XXZ} + \chi_{XZX} + \chi_{ZXX})$$

In this equation, $\rho(\theta_0)$ is the molecular surface density

$$\chi_T = \sqrt{\chi_X + \chi_Y + \chi_Z} \tag{33}$$

$$\beta_z^{exp} = \frac{\chi_T}{f^2(\omega)\, f(2\omega)\, \rho(\theta_0)} \tag{34}$$

dependent on the anchoring angles:

$$\rho(\theta_0) = \frac{N}{A(\sin\theta_0)} \tag{35}$$

A is the contact surface of the molecule, and N is the number of layers. Local field correction factors $f(\omega)$ and $f(2\omega)$ are given by[33]

$$f(\omega) = \frac{n(\omega)^2 + 2}{3} \qquad f(2\omega) = \frac{n(2\omega)^2 + 2}{3} \tag{36}$$

The values for $n(\omega)$ and $n(2\omega)$ were 1.5 and 1.4, respectively. The refractive indices and thickness d of the film are simultaneously determined by ellipsometry.

6.2. Comparison of Theoretical and Experimental β. A comparison of the calculated and measured z components of the hyperpolarizabilities for the different models is presented in Table 1. For the other components, the comparison is meaningless because they cannot be observed experimentally. The hyperpolarizability values obtained for the monomer−surface system and the dimer are too close; therefore, the dominant optical response could not be assigned to either type of association in a conclusive way. The solution to this problem comes from the ellipsometric results. As shown in Table 1, the thickness of the layers, d, permits us to identify the number of layers. Consistency with both set of data requires that the experimental value for β_z be interpreted as arising from the response of the dimer. This interpretation does not neglect the importance of the surface−adsorbate interaction: this is essential to break the symmetry, to induce the resulting geometry, and to activate the components of the hyperpolarizability tensor with nonzero contributions along the surface plane. For small clusters, one gets responses associated with null components of the susceptibility, but these spurious responses vanish as the size of the cluster increases.

A charge-transfer mechanism, coupled to the low-lying SHG transitions, seems to be involved in both the surface−monomer and dimer responses. This can be seen in the orientation of the SOMO and LUMO orbitals either in the direction toward the surface or in direction toward the other member of the dimer, as seen in Figure 8.

7. Conclusions

Using a hybrid quantum classical description that relies on an extended semiempirical approach to the description of the electronic structure of adsorbate−cluster systems, we have provided a consistent description of the optical response of VOOETP on glass surfaces. Such a description includes experimental information and educated theoretical modeling, which can, in principle, be extended to other porphyrinic systems.

The methodology also provides a way to reduce substantially the amount of experimental information needed to obtain the relevant observables, via a Fourier analysis and subsequent manipulation of a simple novel relationship between the expansion coefficients. Our analysis indicates that the dominant

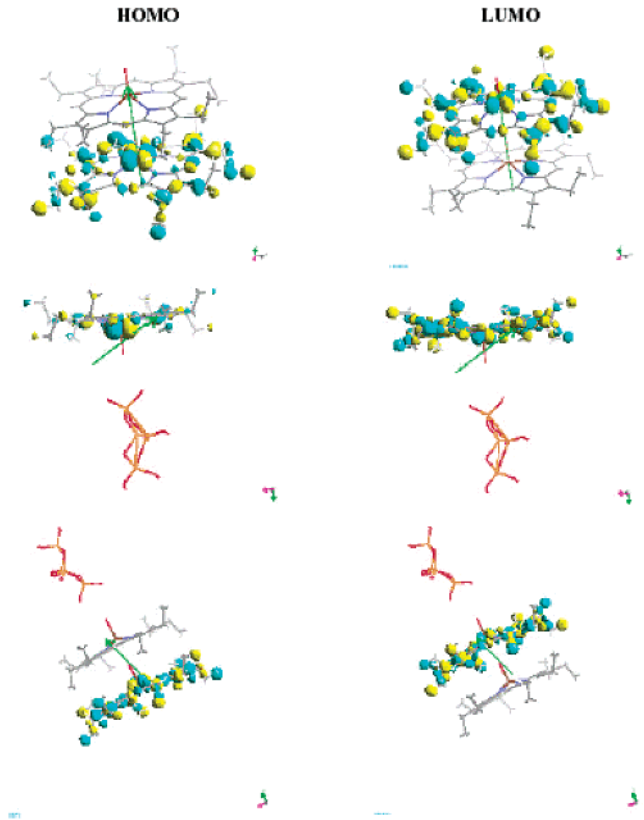

Figure 8. HOMO and LUMO molecular orbitals for the different model systems.

species is the dimer and that the surface plays mostly an orienting role of the adsorbate through a hydrogen bond-induced anchoring. This conclusion is borne out by independent ellipsometry studies that provide information about the thickness of the adsorbate layer. The dominant mechanism, as reported earlier by Ratner and co-workers, seems to involve a charge-transfer mechanism coupled to the low-lying transitions, a situation that can be adequately represented by a sum-over-states approach to the hyperpolarizability.

Acknowledgment. This work was supported by grants FONACIT G-97000722, G-97000593, CDCH-UCV PG-03-12-4546-1999, and PG-03-12-4031-2000. We gratefully acknowledge the facilities provided by Professor Aristides Marcano (IVIC) for the ellipsometric measures.

Supporting Information Available: Fourier coefficients for the fitting to the experimental data. See eqs 14 and 18 for case I. This material is available free a charge via the Internet at http://pubs.acs.org.

References and Notes

(1) Suslick, K. S.; Rakow, N. A.; Kosal, M.; Chou, J. *J. Porphyrins Phthalocyanines* **2000**, *4*, 407.

(2) Kadish, K.; Smith, K.; Guilard, R. *The Porphyrin Handbook*; Academic Press: New York, 2000; Vol. 6, Chapter 41, pp 43−131.

(3) Caga, I. T.; Carnell, I. D.; Winterbottom, J. M. *J. Chem. Technol. Biotechol.* **2001**, *76*, 179.

(4) Brown, F.; Parks, R. E.; Sleeper, A. M. *Phys. Rev. Lett.* **1965**, *14*, 1029.

(5) Higgins, D. A.; Abrams, M. B.; Byerly, S. K.; Corn, R. M. *Langmuir* **1992**, *8*, 1994.

(6) Eisenthal, K. B. *Chem. Rev.* **1996**, *96*, 1343.

(7) Di Bella, S.; Fragalà, I.; Marks, T. J.; Ratner, M. A. *J. Am. Chem. Soc.* **1996**, *118*, 12747.

(8) Mujica, V.; Nieto, P.; Puerta, L.; Acevedo, S. *Energy Fuels* **2000**, *14*, 632.

(9) Rappé, A. K.; Casewit, C. J.; Colwell, K. S.; Goddard, W. A., III; Skiff, W. M. *J. Am. Chem. Soc.* **1992**, *114*, 10024.

(10) Rappé, A. K.; Colwell, K. S.; Casewit, C. J. *Inorg. Chem.* **1993**, *32*, 3438.

(11) Molinaro, F. S.; Ibers, J. A. *Inorg. Chem.* **1976**, *15*, 2278.

(12) Zerner, M.; Gouterman, M. *Inorg. Chem.* **1966**, *5*, 1699.

(13) Gouterman, M. *The Porphyrins*: *Physical Chemistry*; Canada, D. D., Ed.; Academic Press: London, 1978; Vol. III, Part A, Chapter 1, p 12.

(14) Albert, I. D. L.; Marks, T. J.; Ratner, M. A. *Chem. Mater.* **1998**, *10*, 753.

(15) Di Bella, S.; Fragalà, I.; Marks, T. J.; Ratner, M. A. *J. Am. Chem. Soc.* **1996**, *118*, 12747.

(16) Computational results obtained using software programs from Molecular Simulations Inc. Electronic Excitations calculations were made with the *ZINDO* program, and graphical displays were printed out from the *Cerius*^{2} *Molecular Modeling System*.

(17) Oliveira, K. M. T.; Trsic, M. *J. Mol. Struct.: THEOCHEM* **1999**, *464*, 289.

(18) Kanis, D. R.; Ratner, M. A.; Marks, T. J. *Chem. Rev.* **1994**, *94*, 195.

(19) Ward, J. F. *Rev. Mod. Phys.* **1965**, *37*, 1.

(20) Botek, E.; Champagne, B. *Appl. Phys. B* **2002**, *74*, 627.

(21) Atkins, P. W. *Quanta: A Handbook of Concepts*, 2nd ed.; Oxford University Press: New York, 1991; p 48.

(22) Shen, R. *The Principles of Nonlinear Optics*; Wiley & Sons: New York, 1984; Chapter 25.

(23) Felderhof, B. U.; Bratz, A.; Marowsky, G.; Roders, O.; Sieveredes, F. *J. Opt. Soc. Am. B* **1993**, *10*, 1824.

(24) Geiger, F.; Stolle, R.; Marowsky, G.; Palenberg, M.; Felderhof, B. U. *Appl. Phys. B* **1995**, *61*, 135.

(25) Chen, S. H.; Frank, C. W. *Langmuir* **1989**, *5*, 978.

(26) Carim, A. H.; Dovek, M. M.; Quate, C. F.; Sinclair, R.; Vorst, C. *Science* **1987**, *237*, 630.

(27) Tillman, N.; Ulman, A.; Penner, T. L. *Langmuir* **1989**, *5*, 101.

(28) Tillman, N.; Ulman, A.; Schildkraut, J. S.; Penner, T. L. *J. Am. Chem. Soc.* **1988**, *110*, 6136.

(29) Wasserman, S. R.; Whitesides, G. M.; Tidswell, I. M.; Ocko, B. M.; Pershan, P. S.; Axe, J. D. *J. Am. Chem. Soc.* **1989**, *111*, 5852.

(30) Mazely, T. L.; Hetherington, W. M., III. *J. Chem. Phys.* **1987**, *86*, 3640.

(31) Jerphagnon, J.; Kurtz, S. K. *J. Appl. Phys.* **1970**, *41*, 1667.

(32) Kimura-Suda, H.; Sassa, T.; Wada, T.; Sasabe, H. *J. Phys. Chem. B* **2001**, *105*, 1763.

(33) Liu, Y.; Hu, W.; Xu, Y.; Liu, S.; Zhu, D. *J. Phys. Chem. B* **2000**, *104*, 11859.